Electron mobility in InN and III-N alloys

L. Hsu, R. E. Jones, S. X. Li, K. M. Yu, and W. Walukiewicz

Citation: Journal of Applied Physics **102**, 073705 (2007); doi: 10.1063/1.2785005
View online: http://dx.doi.org/10.1063/1.2785005
View Table of Contents: http://scitation.aip.org/content/aip/journal/jap/102/7?ver=pdfcov
Published by the AIP Publishing

Electron mobility in InN and III-N alloys

L. Hsu
Department of Postsecondary Teaching and Learning, University of Minnesota, Minneapolis, Minnesota 55455, USA

R. E. Jones and S. X. Li
Electronic Materials Program, Materials Sciences Division, Lawrence Berkeley National Laboratory, Berkeley, California 94720, USA and Department of Materials Science and Engineering, University of California, Berkeley, California 94720, USA

K. M. Yu and W. Walukiewicz[a)]
Electronic Materials Program, Materials Sciences Division, Lawrence Berkeley National Laboratory, Berkeley, California 94720, USA

(Received 3 July 2007; accepted 3 August 2007; published online 3 October 2007)

We have calculated electron mobilities in InN and its III-nitride alloys using a variational procedure and taking into account the standard scattering mechanisms of Coulomb scattering, alloy disorder, and optical and acoustic phonons. The effects of the nonparabolicity of the conduction band and resulting energy-dependent effective mass have also been included. Scattering from charged Coulombic centers and alloy disorder are the dominant scattering mechanisms that limit the mobilities in currently available materials. Phonons play a role only in relatively pure ($n < 10^{18}$ cm^{-3}) samples or at very high temperatures ($T > 400$ K). In addition, our calculations are in good agreement with experimental Hall mobilities obtained through controlled doping studies performed on InN, InGaN, and InAlN by high energy irradiation. © *2007 American Institute of Physics*. [DOI: 10.1063/1.2785005]

I. INTRODUCTION

The discovery of the low band gap of InN (Refs. 1 and 2) has led to intensive studies of the electronic properties of In-rich group III-nitride alloys. The potential for tuning the direct band gap between 0.7 and 6.2 eV has opened up the possibility of using III-nitride materials in optoelectronic applications ranging from the infrared to the ultraviolet. The electronic structure of the conduction band of group III-nitride alloys is now quite well established.[3] However, much less progress has been made in understanding the electrical properties of In-rich group III-nitride alloys. The reason for this is the presence of an *n*-type conducting surface layer in $In_{1-x}Ga_xN$ with $x < 0.65$ and $In_{1-y}Al_yN$ with $y < 0.36$. The contribution of the surface layer to the total conductivity can make the interpretation of electrical measurements difficult.

Recently, better techniques have allowed the growth of single crystal InN with a low defect density and electron concentrations near 10^{17} cm^{-3}. In addition, it has been shown that bulk InN with reproducibly controlled carrier densities from 10^{18} cm^{-3} up to nearly 10^{21} cm^{-3} can be achieved through irradiation with high energy H^+ and He^+ ions.[4] These samples have shown excellent transport properties at room temperature. The availability of experimental data enables us to investigate theoretically the transport properties of InN. In the mid-1990s, when interest in the nitride materials first exploded, some calculations were published estimating electron mobilities in InN and its alloys.[5,6] However, at that time, the physical properties of the nitrides were not well characterized and material properties not well known. In addition, there was little experimental data with which to compare theoretical predictions.

In this paper, we present results of theoretical calculations of the electron mobility in group III-nitride compounds and their alloys using recently determined materials parameters. The calculations include all the major electron-scattering processes and, in addition, account for the nonparabolicity of the conduction band of InN and In-rich alloys. The results are compared directly with experimental data.

II. BAND STRUCTURE AND MOBILITY CALCULATIONS

The small energy gap of InN and In-rich group III-nitride alloys leads to a strong $\mathbf{k}\cdot\mathbf{p}$ interaction between the *s*-like states of the conduction band and the *p*-like states of the valence band. As a result of the interaction, the electronic states in the conduction band are a mixture of *s*-type and *p*-type wave functions. In addition, the dispersion relation of the conduction band is no longer parabolic, but is rather described by the function

$$E(k) = \sqrt{\left(\frac{E_g}{2}\right)^2 + E_g\frac{\hbar^2k^2}{2m_0^*}} - \frac{E_g}{2}, \tag{1}$$

where k is the electron wave vector, E_g is the band gap, and m_0^* is the effective electron mass at the conduction band minimum.[7] Equation (1) does not include the free electron term ($\nabla^2k^2/2m_0$), which is negligible for small k. The two-band $\mathbf{k}\cdot\mathbf{p}$ treatment used to derive Eq. (1) breaks down when interactions with higher bands become significant. For the purposes of this paper, the two band treatment is always

a)Electronic mail: w_walukiewicz@lbl.gov

valid because the higher bands are well above the highest energies considered here. For example, Furthmüller *et al.* have calculated the next lowest conduction band minimum in InN to be 2.5–3.0 eV above the minima at the Γ point.[8] This dispersion relation leads to an energy-dependent effective mass that increases with increasing energy

$$m^* = \hbar^2 k \left(\frac{dE}{dk} \right)^{-1} = m_0^* \left(1 + 2\frac{E}{E_g} \right). \tag{2}$$

To calculate the electron mobilities, we use a standard variational method[9,10] modified to take into account the nonparabolicity of the conduction band. We include the standard mechanisms of acoustic phonons, polar optical phonons, Coulomb, and alloy disorder scattering. In the calculations we have used the expressions for scattering in the zinc blende rather than the wurtzite crystal structure as they are readily available. However, it has been shown that the numerical results for the two crystal structures do not differ significantly.[11]

The mathematical expressions for the scattering rates due to various mechanisms in small-gap materials with a nonparabolic conduction band are similar to those for materials with a parabolic conduction band, and in some cases differ only by the presence of additional form factors that account for the mixed nature of the conduction band wave functions. However, as we shall see, the addition of these form factors can have a large effect on the numerical results, especially at large carrier concentrations where the effects of the nonparabolicity are most evident.

Carrier scattering by acoustic phonons occurs through both the deformation potential and piezoelectric modes. The relaxation time for the deformation potential mode is

$$\tau_{\mathrm{def}} = \frac{\pi \hbar^3 \rho}{k_B T E_1^2 m^* k} \left(\frac{F_{\mathrm{ac}}^{\parallel}}{v_{\parallel}^2} + \frac{F_{\mathrm{ac}}^{\perp}}{v_{\perp}^2} \right)^{-1}, \tag{3}$$

where ρ is the density of the material, E_1 is the deformation potential, $v_{\parallel}$ and $v_{\perp}$ are the longitudinal and transverse phonon velocities, and $F_{\mathrm{ac}}^{\parallel}$ and $F_{\mathrm{ac}}^{\perp}$ are energy-dependent form factors.[7] The relaxation time for piezoelectric mode scattering is

$$\tau_{\mathrm{pie}} = \frac{\hbar^3 \rho \varepsilon^2 k}{4\pi e^2 e_{14}^2 k_B T m^*} \left(\frac{F_{\mathrm{pie}}^{\parallel}}{v_{\parallel}^2} + \frac{F_{\mathrm{pie}}^{\perp}}{v_{\perp}^2} \right)^{-1}, \tag{4}$$

where ε is the dielectric constant, e_{14} is one of the elements in the piezoelectric tensor, and $F_{\mathrm{pie}}^{\parallel}$ and $F_{\mathrm{pie}}^{\perp}$ are again energy-dependent form factors.[7]

Coulomb scattering by charged impurities has a relaxation time given by

$$\tau_{\mathrm{Coul}} = \sum_i \frac{\varepsilon^2 \hbar^3 k^3}{2\pi m^* e^4 N_i Z_i^2 F_{\mathrm{imp}}}, \tag{5}$$

with the form factor F_{imp} given in Ref. 12 and where N_i and Z_i are the densities and charge states of each of the different species of charged centers i found in the material.

Finally, the relaxation time for scattering by alloy disorder is given by

$$\tau_{\mathrm{alloy}} = \frac{\pi \hbar^3}{kx(1-x) N_{\mathrm{sites}} V^2 F_{\mathrm{all}}}, \tag{6}$$

where N_{sites} is the number of sites per unit volume of the cation sublattice, x is the alloy fraction, F_{all} is a form factor, and V is related to the difference between the atomic potentials of the two different cations.[13] Although the precise value of V can only be calculated if one knows the atomic potentials of the two types of cations, for the calculations in this paper, we used the energy of the conduction band offset between the two corresponding binary III-N semiconductors as the value of V. As with most treatments of scattering in bulk semiconductors, we have neglected free-carrier screening of this mechanism because alloy disorder is the result of short-range potential fluctuations.

Because scattering by optical phonons is an inelastic process, one cannot define a corresponding relaxation time for this mechanism. The total mobility taking into account all of the mechanisms described earlier including optical phonons can be calculated through a variational principle method[10]

$$\mu = -\frac{1}{3\pi^2 n} \frac{D_{3/2,3/2}}{D}, \tag{7}$$

where

$$D_{3/2,3/2} = \begin{vmatrix} 0 & \beta_0^{(3/2)} & \beta_1^{(3/2)} & \cdots \\ \beta_0^{(3/2)} & d_{00} & d_{01} & \cdots \\ \beta_1^{(3/2)} & d_{10} & d_{11} & \cdots \\ \cdots & \cdots & \cdots & \cdots \end{vmatrix},$$

$$D = \begin{vmatrix} d_{00} & d_{01} & \cdots \\ d_{10} & d_{11} & \cdots \\ \cdots & \cdots & \cdots \end{vmatrix},$$

with

$$\beta_i^{(3/2)} = \int_0^{\infty} \left(-\frac{\partial f_0}{\partial E} \right) \left(\frac{E}{k_B T} \right)^i k^3 dE,$$

$$d_{ij} = \int_0^{\infty} \left(-\frac{\partial f_0}{\partial E} \right) \left(\frac{E}{k_B T} \right)^i L_j k^3 dE,$$

$$L_j = \frac{m^*}{e} \left[F_{\mathrm{PO}} + \left(\frac{E}{k_B T} \right)^j \sum_s \frac{1}{\tau_s} \right].$$

In the earlier expressions, n is the carrier density, f_0 is the Fermi–Dirac distribution function $f_0 = \{1 + \exp[(E - E_F)/k_B T]\}^{-1}$, F_{PO} is a form factor for polar optical phonon scattering,[7] and the summation in L_j is performed over all included elastic scattering mechanisms. Although the matrices $D_{3/2,3/2}$ and D are in principle, infinite, using only the elements in the first four rows and columns is sufficient to obtain results accurate to within a few percent. Table I shows the values of the parameters used in the calculations.

TABLE I. Materials parameters used in the mobility calculations. Unless otherwise noted, all values come from Ref. 20.

Parameter		InN	GaN	AlN
Band gap (eV)		0.7[a]	3.4	6.2
Spin-orbit splitting (meV)		3	8	19
Effective mass (band edge) (m_0)		0.07[a]	0.2	0.4
Dielectric constant	Static	9.3[b]	8.9	8.5
	High frequency	6.7[c]	5.35	4.6
Optical phonon energy (meV)		73	91.2	99.2
Acoustic phonon velocity	Longitudinal (10^5 cm/s)	5.2	8	11.1
	Transverse (10^5 cm/s)	1.2	4.1	6.2
Piezoelectric constant e_{14}(C/m^2)		0.375[d]	0.375[d]	0.375[d]
Deformation potential (eV)		3.6[e]	9.1[f]	9.5[g]
Density (g/cm^3)		6.81	6.15	3.23
Conduction band offset relative to InN (eV)		⋯	1.7[h]	3.8[h]

[a]Reference 3.
[b]Derived from the Lyddane–Sachs–Teller relation and the high-frequency dielectric constant with phonon frequencies from Ref. 14.
[c]Reference 15.
[d]Reference 16.
[e]Reference 17.
[f]Reference 18.
[g]Reference 5.
[h]Reference 19.

III. RESULTS AND DISCUSSION

The relative importance of the various electron scattering mechanisms as a function of temperature in a sample of InN with a room temperature electron concentration of 4.4×10^{17} cm^{-3} is shown in Fig. 1. The calculations assume that the electrons originate from singly ionized donors with a compensation ratio of $\theta=0.2$. Experimental data for a sample with the same electron concentration are also shown in this figure. The calculations are in a reasonably good agreement with experiment for temperatures higher than about 150 K indicating good crystal quality since no other scattering mechanisms appear to contribute significantly. At temperatures lower than 150 K the calculated mobility is considerably higher than the data. This indicates that another scattering mechanism may be operational at these low temperatures. One possibility of an additional mechanism is scattering by random electrostatic and strain potentials resulting from dislocations and/or a nonuniform distribution of dopants. Random potential fluctuations are known to contribute to the electron scattering.[21] A distinct strong temperature dependence of the electron mobility is expected in this case.

Figure 2 shows the calculated electron mobilities for various scattering mechanisms as a function of the electron concentration at room temperature. The calculations predict that in InN samples with carrier concentrations above the mid-10^{18} cm^{-3} range, Coulomb scattering by singly ionized donors will be the dominant mechanism. At lower doping levels, scattering by optical phonons and by acoustic phonons via the piezoelectric mode becomes important. Scattering by acoustic phonons through the deformation potential mode is unimportant at any carrier concentration.

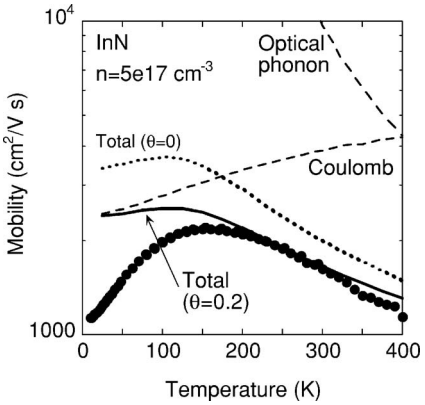

FIG. 1. Electron mobilities in InN as functions of temperature. For a compensation ratio of $\theta=0.2$, the calculated component mobilities are shown with dashed lines and the heavy solid line is the total mobility taking all mechanisms into account. The acoustic phonon component mobilities are too high to be seen on this scale. Experimental points are shown as solid circles. For reference, the total mobility assuming no compensation ($\theta=0$) is also shown.

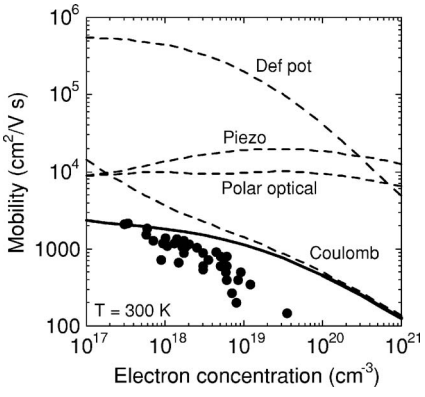

FIG. 2. Electron mobilities in as-grown InN as functions of carrier concentration. The calculated component mobilities are shown with dashed lines and the heavy solid line is the mobility taking all mechanisms into account. Experimental points are shown as solid circles.

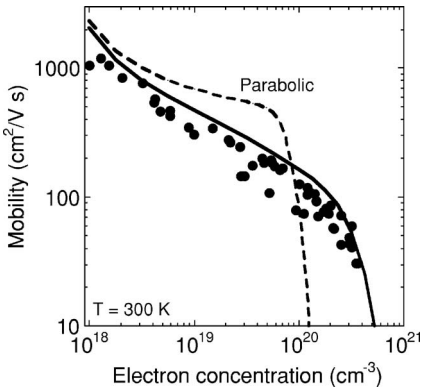

FIG. 3. Calculated and measured electron mobilities in InN after irradiation by 2 MeV H^+ and He^+ ions. The mobility is completely controlled by Coulomb scattering. The scattering centers are assumed to be triply charged native defects with a charge transition level 0.9 eV above the bottom of the InN conduction band. The dashed line shows mobilities calculated assuming a parabolic conduction band.

It has been shown recently that irradiation with 2 MeV He^+ ions can be used for *n*-type doping through the controlled incorporation of native defects.[22,23] As can be seen from the experimental points in Fig. 3, such irradiation has been used for doping up to concentrations in the mid-10^{20} cm^{-3}. Although ion-channeling measurements show that the crystalline quality of the samples remains high after irradiation,[22] Hall effect measurements show that the electron mobilities are much lower than those predicted by the curve calculated for singly ionized charged centers shown in Fig. 2. However, these lower mobility values can be explained quite well if we assume that the native defects produced by irradiation are triply charged Coulomb centers. At the high carrier concentrations shown in this graph, the mobility is limited by Coulomb scattering from the triply charged defects alone. One notable contrast between Figs. 2 and 3 lies in the agreement between the calculated and experimental mobilities at high electron concentrations. In as-grown material with high electron concentrations, the growth conditions likely result in large numbers of structural defects, such as charged, extended dislocations. Because little is known about the exact characteristics of these defects, modeling their influence involves the use of fitting parameters and we have decided to neglect them in our calculations. On the other hand, it is clear from Fig. 3 that irradiation with He^+ ions does not generate many such defects.

Measurements of the carrier concentration as a function of the irradiation fluence suggest that the defects are amphoteric in nature, with the ratio of donor to acceptor defects determined by the relative positions of the Fermi level E_F and the Fermi level stabilization energy E_{FS} in the InN material.[24–26] In InN, E_{FS} is about 0.9 eV above the conduction band minimum and coincides with the charge transition state of the defects produced by irradiation. When E_F is below E_{FS}, it is energetically favorable for the defect to assume a donor configuration because the donated electrons will drop from the higher energy charge transition level at E_{FS} to the lower energy Fermi level E_F, reducing the effective formation energy by the energy difference between the two levels multiplied by the charged state of the donor. The effective formation energy of acceptors is increased for the same reason. Thus, the concentrations of donors N_D and acceptors N_A are given by

$$N_D = N_{\text{sites}} \exp\left\{\frac{-[E_{fD}^0 - 3(E_{FS} - E_F)]}{k_B T}\right\},$$

$$N_A = N_{\text{sites}} \exp\left\{\frac{-[E_{fA}^0 - 3(E_F - E_{FS})]}{k_B T}\right\}, \tag{8}$$

where N_{sites} is the concentration of defect sites and E_{fD}^0 and E_{fA}^0 are the unperturbed formation energies of the donor and acceptor defect configurations. The factor of 3 is present because we assume that both the donors and acceptors are triply charged.

In the amphoteric defect model because the formation energies of donor and acceptor defects are equal when $E_F = E_{FS}$, E_{fD}^0, and E_{fA}^0 are equal and thus an effective compensation ratio θ_0 and electron concentration n can be calculated from

$$\theta_0 = \frac{N_A}{N_D} = \exp\left[\frac{-6(E_{FS} - E_F)}{k_B T}\right] \tag{9}$$

and $n = 3N_D - 3N_A$.

Equation (9) gives the compensation ratio under ideal circumstances, with an infinitely sharp defect charge transition state energy. However, the large concentration of defects causes interaction between the defect energy levels. The degree of interaction varies due to some spatial variation in the defect distribution, and thus the defect charge transition state energy is broadened. To phenomenologically model this inhomogeneous broadening and obtain a more realistic value for the compensation ratio θ, we convoluted θ_0 with a Gaussian function

$$\theta = \frac{1}{\Delta\sqrt{\pi}} \int_{-\infty}^{\infty} \exp\left[\frac{-6(E' - E_F)}{k_B T}\right] \times \exp\left[-\left(\frac{E' - E_{FS}}{\Delta}\right)^2\right] dE', \tag{10}$$

where Δ is the broadening parameter. In all of the calculations in this paper, we used a value of $\Delta = 0.22$ eV, consistent with the value found from fitting to the absorption spectra of InGaN.[22]

The theoretical mobilities in Fig. 3 were calculated assuming a single donor concentration of 10^{18} cm^{-3} (impurities present in the as-grown sample) and the concentrations of triple donors and acceptors necessary to produce the measured net carrier concentration. Because of the near-exponential dependence of the compensation ratio, the concentration of native acceptor defects remains negligible until E_F comes very close to E_{FS}, near a carrier concentration of 4×10^{20} cm^{-3}. The sudden drop in mobility values at this point arises from the sharp increase in the number of charged native acceptor defects and a corresponding increase in the efficiency of scattering due to the presence of many more charged Coulomb centers.

Figure 3 also presents an opportunity to view the effects of the nonparabolic conduction band. The dashed line shows

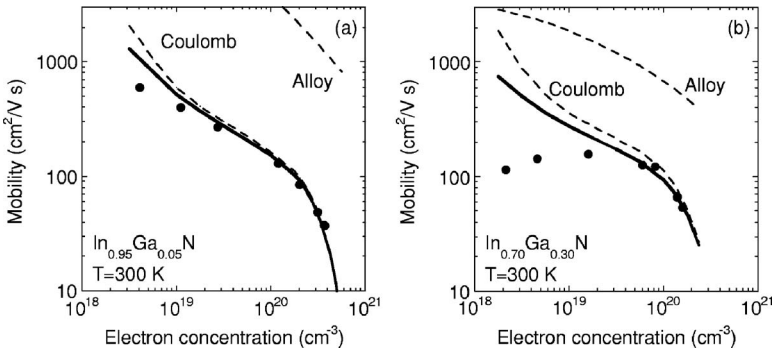

FIG. 4. Calculated and measured electron mobilities in InGaN after irradiation by 2 MeV He^+ ions. Results for two different alloy compositions are shown including (a) 5% Ga and (b) 30% Ga. The Coulomb scattering centers are assumed to be triply charged native defects with a charge transition level resonant with the conduction band. The dashed lines show the component mobilities due to Coulomb scattering and alloy disorder scattering.

the theoretical mobilities assuming a standard parabolic conduction band. It is clear that the decrease in mobility with increasing electron concentration predicted by a parabolic conduction band model is much less rapid than what is observed experimentally. In addition, because of the smaller average density of states, fewer electrons can be accommodated in the conduction band before E_F reaches E_{FS}, leading to an incorrect prediction of the carrier concentration at which the mobilities experience a sharp decrease due to increased formation of native acceptor defects.

In Figs. 4 and 5, we compare our calculations with experimental results for irradiated InGaN and InAlN alloys with different compositions. As with pure InN, the general shape of the mobility curves can be explained by Coulomb scattering from triply charged native donors defects produced by the irradiation and the Fermi stabilization model. The position of the Fermi stabilization level E_{FS} relative to the conduction band minimum depends on the alloy composition x and is given by

$$E_{FS}(x) = 0.9 \text{ eV} - \frac{\text{CB}_{\text{GaN}} - \text{CB}_{\text{InN}}}{E_{g\ \text{GaN}} - E_{g\ \text{InN}}}(E_{g\ \text{InGaN}} - E_{g\ \text{InN}}) \tag{11}$$

for InGaN alloys and the corresponding expression for InAlN alloys. In this expression, $\text{CB}_{\text{GaN}} - \text{CB}_{\text{InN}}$ is the conduction band offset between InN and GaN and E_g are the band gaps. Thus, on an absolute scale, the defect level is independent of the alloy composition and it is the energy of the conduction band minimum that shifts with alloying. The Fermi stabilization energy is reduced from its value of 0.9 eV in pure InN by an amount equal to the alloy induced shift in the conduction band energy. We use values of 1.7 and 3.8 eV for the InN/GaN and InN/AlN conduction band offsets, respectively.[27]

At low electron concentrations, the experimental points in Figs. 4 and 5 have, in general, lower mobilities than are predicted by our calculations. One possible explanation for this divergence is a nonuniformity in the distribution of the two different types of cations in the lattice, which would result in increased carrier scattering. This effect would be more apparent at low electron concentrations because the

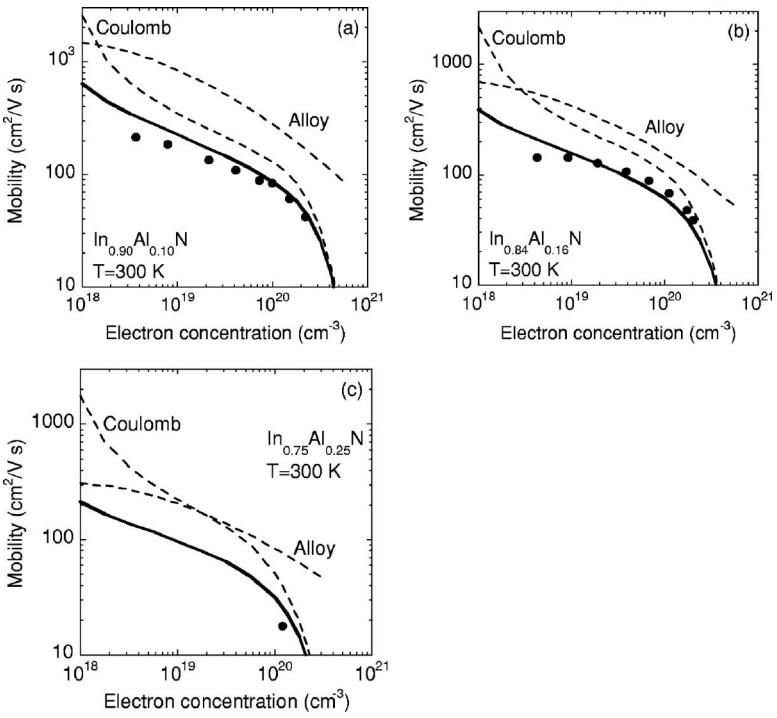

FIG. 5. Calculated and measured electron mobilities in InAlN after irradiation by 2 MeV He^+ ions. Results for three different alloy compositions are shown including (a) 10% Al, (b) 16% Al, and (c) 25% Al. The Coulomb scattering centers are assumed to be triply charged native defects with a charge transition level resonant with the conduction band. The dashed lines show the component mobilities due to Coulomb scattering and alloy disorder scattering.

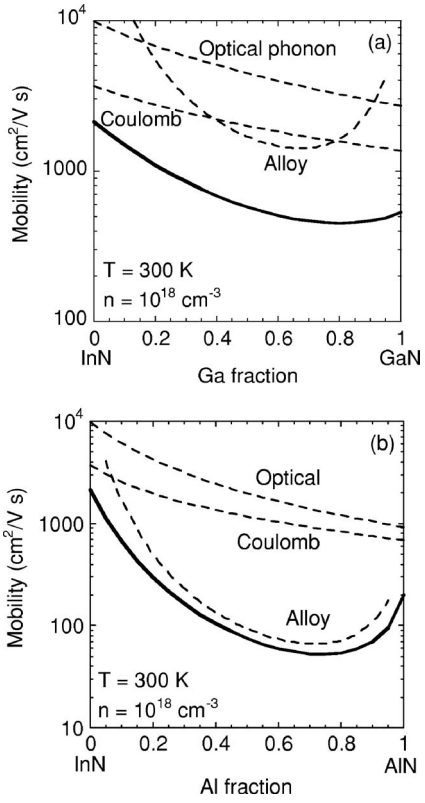

FIG. 6. Calculated electron mobilities as a function of alloy composition in (a) InGaN and (b) InAlN. The Coulomb scattering centers are assumed to be singly charged hydrogenic impurities.

potential variations would be less efficiently screened by free carriers. However, this effect is difficult to estimate quantitatively as the size and the magnitude of the potential fluctuations are not known.

Finally, Fig. 6 shows calculated mobilities in as-grown $In_{1-x}Ga_xN$ and $In_{1-x}Al_xN$ as a function of alloy composition for an electron concentration of 1×10^{18} cm^{-3}. The scattering by acoustic phonons is unimportant compared to the mechanisms shown. As one might expect, alloy disorder scattering is much more important in $In_{1-x}Al_xN$ because of the much larger offset between the InN and AlN conduction bands, than between the conduction bands of InN and GaN. In these calculations, the Coulomb scattering centers were assumed to be ordinary singly charged hydrogenlike impurities, rather than the triply charged defects we assumed in the irradiated samples.

IV. SUMMARY

We have calculated electron mobilities in InN and its alloys with GaN and AlN. In pure InN, Coulomb scattering from charged centers is the dominant mobility-limiting mechanism in the majority of cases, though scattering from polar optical phonons and piezoelectric mode acoustic phonons becomes important at the lowest doping concentrations ($<10^{18}$ cm^{-3}) and at very high temperatures. In the InGaN and InAlN alloys, Coulomb and alloy disorder scattering are the dominant processes. Our calculations agree reasonably well with experimental data and also suggest that the defects resulting from irradiation of InN and its III-nitride alloys are triply charged donors. At the highest electron concentrations produced by irradiation, the Fermi stabilization energy model predicts an increase in the compensation ratio of the irradiation-generated defects, leading to a sudden decrease in the mobilities.

ACKNOWLEDGMENTS

This work was supported in part by the Director, Office of Science, Office of Basic Energy Sciences, Division of Materials Sciences and Engineering, of the U.S. Department of Energy under Contract No. DE-AC02-05CH11231. R.E.J. acknowledges support from a National Defense Science and Engineering Graduate fellowship. The authors would like to thank Bill Schaff for providing the samples that were irradiated.

[1] V. Yu. Davydov, A. A. Klochikhin, R. P. Seisyan, V. V. Emtsev, S. V. Ivanov, F. Bechstedt, J. Furthmüller, H. Harima, A. V. Mudryi, J. Aderhold, O. Semchinova, and J. Graul, Phys. Status Solidi B **229**, R1 (2002).
[2] J. Wu, W. Walukiewicz, K. M. Yu, J. W. Ager III, E. E. Haller, H. Lu, W. J. Schaff, Y. Saito, and Y. Nanishi, Appl. Phys. Lett. **80**, 3967 (2002).
[3] W. Walukiewicz, J. W. Ager III, K. M. Yu, Z. Liliental-Weber, J. Wu, S. X. Li, R. E. Jones, and J. D. Denlinger, J. Phys. D **39**, R83 (2006).
[4] R. E. Jones, S. X. Li, L. Hsu, K. M. Yu, W. Walukiewicz, Z. Liliental-Weber, J. W. Ager III, E. E. Haller, H. Lu, and W. J. Schaff, Physica B (Amsterdam) **376–377**, 436 (2006).
[5] V. W. L. Chin, T. L. Tansley, and T. Osotchan, J. Appl. Phys. **75**, 7365 (1994).
[6] V. W. L. Chin, B. Zhou, T. L. Tansley, and X. Li, J. Appl. Phys. **77**, 6064 (1995).
[7] W. Szymanska and T. Dietl, J. Phys. Chem. Solids **39**, 1025 (1978).
[8] J. Furthmüller, P. H. Hahn, F. Fuchs, and F. Bechstedt, Phys. Rev. B **72**, 205106 (2005).
[9] D. J. Howarth and E. H. Sondheimer, Proc. R. Soc. London, Ser. A **219**, 53 (1953).
[10] W. Walukiewicz, L. Lagowski, L. Jastrzebski, M. Lichtensteiger, and H. C. Gatos, J. Appl. Phys. **50**, 899 (1979).
[11] B. C. Lee, K. W. Kim, M. Dutta, and M. A. Stroscio, Phys. Rev. B **56**, 997 (1997).
[12] W. Zawadzki and W. Szymanska, Phys. Status Solidi B **45**, 415 (1971).
[13] J. Kossut, Phys. Status Solidi B **86**, 593 (1978).
[14] V. Yu. Davydov and A. A. Klochikhin, Semiconductors **38**, 861 (2004).
[15] T. Inushima, T. Shiraishi, and V. Yu Davydov, Solid State Commun. **110**, 491 (1999).
[16] M. Shur, B. Gelmont, and M. Asif Khan, J. Electron. Mater. **25**, 777 (1996).
[17] S. X. Li, J. Wu, E. E. Haller, W. Walukiewicz, W. Shan, H. Lu, and W. J. Schaff, Appl. Phys. Lett. **83**, 4963 (2003).
[18] W. Knap, E. Borovitskaya, M. S. Shur, L. Hsu, W. Walukiewicz, E. Frayssinet, P. Lorenzini, N. Grandjean, C. Skierbiszewski, P. Prystawko, M. Leszczynski, and I. Grzegory, Appl. Phys. Lett. **80**, 1228 (2002).
[19] J. Wu and W. Walukiewicz, Superlattices Microstruct. **34**, 63 (2003).
[20] *Properties of Advanced Semiconductor Materials GaN, AlN, InN, BN, SiC, SiGe*, edited by M. E. Levinshtein, S. L. Rumyantsev, and M. S. Shur (Wiley, New York, 2001).
[21] J. Wu, K. W. Yu, W. Walukiewicz, G. He, E. E. Haller, D. E. Mars, and D. R. Chamberlin, Phys. Rev. B **68**, 195202 (2003).
[22] S. X. Li, E. E. Haller, K. M. Yu, W. Walukiewicz, J. W. Ager III, J. Wu, W. Shan, H. Lu, and W. J. Schaff, Appl. Phys. Lett. **87**, 161905 (2005).
[23] R. E. Jones, K. M. Yu, S. X. Li, W. Walukiewicz, J. W. Ager III, E. E. Haller, H. Lu, and W. J. Schaff, Phys. Rev. Lett. **96**, 125505 (2006).
[24] G. A. Baraff and M. Schlüter, Phys. Rev. Lett. **55**, 1327 (1985).
[25] W. Walukiewicz, Appl. Phys. Lett. **54**, 2094 (1989).
[26] W. Walukiewicz, Physica B (Amsterdam) **302–303**, 123 (2001).
[27] G. Martin, A. Botchkarev, A. Rockett, and H. Morkoç, Appl. Phys. Lett. **68**, 2541 (1996).